# Journal Pre-proof

White matter fiber density abnormalities in cognitively normal adults at risk for late-onset Alzheimer´s disease.

Stella M. Sánchez, Bárbara Duarte-Abritta, Carolina Abulafia, Gabriela De Pino, Hernan Bocaccio, Mariana N. Castro, Gustavo E. Sevlever, Greg A. Fonzo, Charles B. Nemeroff, Deborah R. Gustafson, Salvador M. Guinjoan, Mirta F. Villarreal

| | |
|---|---|
| PII: | S0022-3956(19)31029-5 |
| DOI: | https://doi.org/10.1016/j.jpsychires.2019.12.019 |
| Reference: | PIAT 3804 |
| To appear in: | *Journal of Psychiatric Research* |
| Received Date: | 02 December 2019 |
| Accepted Date: | 30 December 2019 |

Please cite this article as: Stella M. Sánchez, Bárbara Duarte-Abritta, Carolina Abulafia, Gabriela De Pino, Hernan Bocaccio, Mariana N. Castro, Gustavo E. Sevlever, Greg A. Fonzo, Charles B. Nemeroff, Deborah R. Gustafson, Salvador M. Guinjoan, Mirta F. Villarreal, White matter fiber density abnormalities in cognitively normal adults at risk for late-onset Alzheimer´s disease., *Journal of Psychiatric Research* (2019), https://doi.org/10.1016/j.jpsychires.2019.12.019

# White matter fiber density abnormalities in cognitively normal adults at risk for late-onset Alzheimer´s disease.

Stella M. Sánchez[a,b,c], Bárbara Duarte-Abritta[a], Carolina Abulafia[a,b,d], Gabriela De Pino[a,e,f], Hernan Bocaccio[a,b,c], Mariana N. Castro[a,b,g,h], Gustavo E. Sevlever[i], Greg A. Fonzo[j], Charles B. Nemeroff[j], Deborah R. Gustafson[k,l], Salvador M. Guinjoan[a,b,g,h,m,n*], Mirta F. Villarreal[a,b,c]

a Grupo de Investigación en Neurociencias Aplicadas a las Alteraciones de la Conducta, Instituto de Neurociencias FLENI-CONICET, Argentina

b Consejo Nacional de Investigaciones Científicas y Técnicas (CONICET), Argentina

c Departamento de Física, Facultad de Cs. Exactas y Naturales, Universidad de Buenos Aires, Argentina

d Institute for Biomedical Research (BIOMED), Pontifical Catholic University of Argentina, Argentina

e Escuela de Ciencia y Tecnología, Universidad Nacional de San Martín, Argentina

f Laboratorio de Neuroimágenes, Departamento de Imágenes, Fundación FLENI, Argentina

g Departamento de Fisiología, Facultad de Medicina, Universidad de Buenos Aires, Argentina

h Departamento de Salud Mental, Facultad de Medicina, Universidad de Buenos Aires, Argentina

i Departamento de Neuropatología y Biología Molecular, Fundación FLENI, Argentina

j Institute of Early Life Adversity Research, Department of Psychiatry, University of Texas at Austin, United States of America

k Department of Neurology, State University of New York University Downstate Medical Center, United States of America

l Department of Health and Education, University of Skövde, Sweden

m Servicio de Psiquiatría, Fundación FLENI, Argentina

n Neurofisiología I, Facultad de Psicología, Universidad de Buenos Aires, Argentina

***Corresponding author**

Salvador M. Guinjoan

Service of Psychiatry, Fleni Foundation

Montañeses 2325 5th floor

C1428AQK Buenos Aires, Argentina

sguinjoan@fleni.org.ar

+54 11 5777 3200 x2514/2531

**Keywords:** Diffusion MRI; white matter microstructure; preclinical late-onset Alzheimer's disease; amyloid deposition; cognitive tests; corpus callosum.

**Abstract**

Tau accumulation affecting white matter tracts is an early neuropathological feature of late-onset Alzheimer's disease (LOAD). There is a need to ascertain methods for the detection of early LOAD features to help with disease prevention efforts. The microstructure of these tracts and anatomical brain connectivity can be assessed by analyzing diffusion MRI (dMRI) data. Considering that family history increases the risk of developing LOAD, we explored the microstructure of white matter through dMRI in 23 cognitively normal adults who are offspring of patients with Late-Onset Alzheimer's Disease (O-LOAD) and 22 control subjects (CS) without family history of AD. We also evaluated the relation of white matter microstructure metrics with cortical thickness, volumetry, in vivo amyloid deposition (with the help of PiB positron emission tomography -PiB-PET) and regional brain metabolism (as FDG-PET) measures. Finally we studied the association between cognitive performance and white matter microstructure metrics. O-LOAD exhibited lower fiber density and fractional anisotropy in the posterior portion of the corpus callosum and right fornix when compared to CS. Among O-LOAD, reduced fiber density was associated with lower amyloid deposition in the right hippocampus, and greater cortical thickness in the left precuneus, while higher mean diffusivity was related with greater cortical thickness of the right superior temporal gyrus. Additionally, compromised white matter microstructure was associated with poorer semantic fluency. In conclusion, white matter microstructure metrics may reveal early differences in O-LOAD by virtue of parental history of the disorder, when compared to CS without a family history of LOAD. We demonstrate that these differences are associated with lower fiber density in the posterior portion of the corpus callosum and the right fornix.

## 1. Introduction

Alzheimer´s disease (AD) is neuropathologically defined in post mortem brain tissue by aggregation of abnormal β-amyloid and hyperphosphorylated Tau proteins. However, extracellular β-amyloid accumulation occurs in up to 80% of elderly people with normal cognition (Aizenstein et al., 2008; Ferrer, 2012), and is not consistently associated with cognitive impairment severity across populations (Boyle et al., 2019; Loewenstein et al., 2018; Rodrigue et al., 2012; Rowe et al., 2010). In contrast, another initiatory pathological process more closely associated with the cognitive deterioration that is characteristic of AD, is believed to be intracellular hyperphosphorylated tau accumulation that primarily affects dendrites and axons (Braak and Del Tredici, 2015). This causes disconnection between different brain regions. In late-onset AD (LOAD), representing approximately 99% of all AD cases, most studies of connectivity using functional (Buckner et al., 2009; Greicius et al., 2004) or structural (Mito et al., 2018) imaging methodology, involve patients with moderate to severe forms of the disorder. To the extent of our knowledge, however, structural connectivity has not been studied in detail in middle-aged, cognitively normal persons at risk for LOAD by virtue of their family history.

Family history increases the risk of developing LOAD (Bertram et al., 2010; Mosconi et al., 2010), and is second only to high age as an epidemiological risk factor. As published previously, persons who are at risk of developing LOAD because of their family history, which can be in part demonstrated by possession of the apolipoprotein E (APOE) ε4 allele, show altered functional and anatomical connectivities (Bendlin et al., 2010; Sánchez et al., 2017; Sheline and Raichle, 2013; Sheng et al., 2017), changes in cognitive variables (Abulafia et al., 2018; Ballard and O'Sullivan, 2013; Loewenstein et al., 2016; Rapp and Reischies, 2005; Reinvang et al., 2012), and abnormal brain structure (Duarte-Abritta et al., 2018; During et al., 2011; Mosconi et al., 2014, 2013; Reiman et al., 2005). In particular, we observed in a sample of offspring of LOAD patients (O-LOAD) that functional connectivity was related to subtle cognitive alterations in episodic memory and the capacity to recover from semantic interference effects during learning when compared to healthy control subjects (CS) (Sánchez et al., 2017). This latter capacity also correlated with brain structure, involving brain regions responsible for autonomic, motor, and motivational control in CS, and regions traditionally implicated in AD in O-LOAD (Abulafia et al., 2018). We also identified isocortical thinning in AD-relevant areas including posterior cingulate, precuneus, and areas of the prefrontal and temporoparietal cortex (Duarte-Abritta et al., 2018).

Anatomical connectivity can be explored through diffusion MRI (dMRI), which is a noninvasive *in vivo* brain imaging method that allows study of white matter (WM) microstructure and reconstruction of fiber trajectories. Classic tensor-derived metrics, such as fractional anisotropy (FA) and mean diffusivity (MD) (Pierpaoli and Basser, 1996) have been applied in AD patients (Bozzali et al., 2002; Kantarci, 2014; Mayo et al., 2017; Ouyang et al., 2015), as well as in preclinical samples including carriers of the APOE ε4 allele and O-LOAD, to study WM integrity (Bendlin et al., 2010; Racine et al., 2014; Ringman et al., 2007). However, these voxel-based metrics are not specific enough for evaluating multiple fiber orientations (i.e., "crossing fibers") and do not identify more subtle anomalies (Pierpaoli et al., 2001). Moreover, crossing fibers are present in approximately 90% of the brain (Jeurissen et al., 2013), where these popular metrics are difficult to interpret and provide no information regarding fiber bundles within a voxel (Douaud et al., 2011; Jones, 2010; Jones et al., 2013). A novel method called fixel-based analysis (FBA) was developed by Raffelt and colleagues (2015) and resolves WM integrity in greater detail, exhibiting within-voxel microstructure, and allowing statistical analysis in complex fiber scenarios.

In the present study, we hypothesized that our sample of 23 cognitively normal, middle-aged (40-60 years) O-LOAD have decreased WM microstructure compared to CS (n=22) without a family history of LOAD. In addition, we tested the hypothesis that FBA could reveal changes of WM integrity in O-LOAD and that such changes would be associated with alterations in gray matter (GM) and clinical cognitive performance (Abulafia et al., 2018; Duarte-Abritta et al., 2018). Regarding the latter point, and based upon prior neuropathological studies across the lifespan (Braak & Braak 1991; Braak and Del Tredici 2015) we predicted that WM integrity would not be topographically related to brain amyloid deposition (as measured by PET-PiB) or neurodegeneration, as evidenced by decreased gray matter volume and cortical thickness.



## 2. Materials and Methods

### 2.1. Participants

Participants were recruited at Fleni Foundation in Buenos Aires, Argentina. The sample included 23 O-LOAD and 22 CS with no known family history of LOAD. All participants provided written informed consent to participate in the study as approved by the local bioethics committee and in accordance with the Declaration of Helsinki. Briefly, the inclusion criterion for O-LOAD was having at least one parent diagnosed with probable LOAD according to DSM-5 criteria. The CS group had no family history of LOAD and neither parent had developed LOAD before age 70. Inclusion criteria for both groups were as follows: (1) 40–60 years of age at the time of enrollment, (2) $\geq$7 years of formal education, (3) Mini Mental State Examination score >26, (4) no evidence of neurologic

disease or medical conditions likely to impair cognitive function, (5) no history of substance abuse (alcohol, marijuana, stimulants, benzodiazepines, or other drugs), and (6) Hachinski score <4 to screen out vascular cognitive disorders.

All participants were asked to provide names, date of birth, age at death, cause of death, and known clinical information for all LOAD-affected family members. The information was confirmed by other family members or by interview with the examining physician, discussing the parents' symptoms and disease progression. Among O-LOAD, at least one parent had been diagnosed with LOAD at age ≥65 years. Details of this sample are described elsewhere (Duarte-Abritta et al., 2018; Abulafia et al., 2019).

### 2.2. MRI data acquisition

MRI data was acquired using a 3T GE Signa HDxt MRI scanner with an eight-channel head coil. Diffusion-weighted images (DWI) was performed using the following parameters: 45 axial slices, 256x256 acquisition matrix, and 0.93x0.93x2.50 $mm^3$ voxel size (TR=12000 ms, TE=88.5 ms), 35 diffusion-weighted images (b=1000 $s/mm^2$) and one volume without diffusion weighting ($b_0$). In addition, conventional high resolution T1 3D fast SPGR-IR images with 166 slices in the sagittal plane, 1.2 mm slice thickness, TR=7.256 ms, TE=2.988 ms, flip angle 8°, FOV=26 cm were acquired.

### 2.3. Positron Emission Tomography (PET) data acquisition

PET image acquisition was performed on a PET/CT General Electric 690. First, 370MBq of $^{11}$C-PiB was administered and, after 50 min, dynamic tomographic images 3D mode were taken in 20 minutes. After 40 min, $^{18}$FDG was administrated and after 30-40 min a new set of dynamic tomographic images in 3D mode were taken during 30 min. Both radiopharmaceuticals were synthesized at Fleni, complying with the pharmaceutical Good Manufacturing Practice standards, and administered doses are those established by the international radiological protection and safety standards. $^{11}$C-PIB and $^{18}$FDG solutions were used to detect the A42 amyloid at extracelular cortical level and to measure neuronal metabolic activity, respectively. Each participant must have been fasting for 6 hours, have a blood glucose level under 130 mg/dl and the procedure is conducted in a quiet dim-lit room.

### 2.4. MRI data preprocessing

The preprocessing of DWI consisted of de-noising the data (Veraart et al., 2016), applying eddy-current and motion correction (Andersson and Sotiropoulos, 2016), and performing bias field correction (Zhang et al., 2001). Subsequently, an intensity normalization across all subjects was

performed by deriving scale factors from the median intensity of selected voxels of WM, GM, and cerebrospinal fluid (CSF) in $b_0$ images. All of these preprocessing steps were performed using MRtrix3 software package. In addition, maps of canonical diffusion metrics, such as FA and MD, were computed using the FSL software package.

T1 image preprocessing consisted of co-registering them to corresponding DWI data using the SPM8 toolbox, extracting the skull using the Brain Extraction Tool (Smith, 2002) as part of FSL software, and generating the tissue-segmented image appropriate for the following processing steps (Patenaude et al., 2011; Smith, 2002; Smith et al., 2004; Zhang et al., 2001). Additionally, co-registered T1 images were parcellated according to Desikan-Killiany atlas (Desikan et al., 2006) implemented in FreeSurfer software as described (Duarte-Abritta et al., 2018).

### 2.5. Diffusion MRI data processing

On DWI preprocessed data, we performed the Constrained Spherical Deconvolution (CSD) model (Tournier et al., 2007) to extract the contribution of WM fiber orientations per voxel (i.e., the fiber orientation distribution FOD) obtaining an image per subject. All FOD images were reached by using a group average response function, applying the multi-shell multi-tissue CSD algorithm (Jeurissen et al., 2014) and, according to the number of diffusion gradients, each FOD was represented by a set of spherical harmonics with a maximum order of 6. Subsequently, a FOD template was performed with twenty subjects of each group, and through non-linear registration each subject's FOD image was taken to the template space.

In the next step, we executed on the FOD template a probabilistic tractography algorithm, where each local WM orientation was connected with the next one delineating the fiber pathways, taking into account the uncertainty derived from errors in the followed trajectory and generating a large distribution of possible pathways from each seed point (Jeurissen et al., 2011; Tournier et al., 2012). We applied the probabilistic iFOD2 algorithm in a whole-brain tractography approach generating 20 million streamlines with seed dynamic option to improve the distribution of reconstructed streamlines density (Smith et al., 2015). In order to reduce reconstruction biases and to provide a more biologically meaningful structural connection density, these streamlines were filtered to 5 million using the spherical deconvolution informed filtering of tractograms (SIFT) (Smith et al., 2013). All processing steps were performed using MRtrix3 package.

### 2.6. Fixel-Based Analysis

WM microstructure was studied mainly using FBA. According to its definition (Raffelt et al., 2015), a fixel refers to a *fi*ber bundle within a vo*xel* and reveals information in a smaller scale than an entire voxel. Three metrics that describe the architecture of WM are derived from FBA: i) fiber

density (FD), the intra-axonal volume of a fiber bundle; ii) fiber-bundle cross-section, number of voxels the fiber bundle occupies by its intra-axonal volume; and iii) fiber density & cross-section that combines both measurements. Performing this method, statistical inference is increased using a General Linear Model and by applying non-parametric permutation testing with 5000 permutations, where family-wise error corrected P-values were assigned to each fixel. All strategies implemented in FBA increase its statistical power and its anatomical interpretation.

In this work, default parameters were used (height increment used in the cfe integration, 0.1; E=2; H=3; c=0.5; Gaussian kernel with the supplied FWHM used to smooth the fixel value along the fiber tracts, 10mm), and using 5 million streamlines tractogram template. This analysis was performed using a computing cluster of the Centro de Cómputos de Alto Rendimiento (CeCAR; https://cecar.fcen.uba.ar/). We selected streamlines from the tractogram template, that were associated to significant fixels (corrected $p<0.05$), and a “significant tract” was obtained. Scripts and commands necessaries for this analysis are part of MRtrix3 package and complete description are published (Raffelt et al., 2017).

### 2.7. Assessment of canonical diffusion tensor-derived metrics

As was described in Section 1, usually diffusion tensor-derived metrics are not specific enough to reveal subtle differences when they are applied in a whole-brain approach, especially in samples with similar characteristics as our O-LOAD and CS groups. We thus decided to use the output of FBA to study FA and MD values only in the area determined by the significant tract. To compare WM integrity between groups through these canonical metrics, we made a mask of this tract and extracted the values corresponding to voxels associated with both metrics. Thus, one score was obtained per subject per metric.

### 2.8. Anatomical connectome

An anatomical connectome was performed, which involves only connections belonging to the significant tract and their associated GM areas.

### 2.9. Neuropsychological assessments

The neuropsychological assessments included semantic fluency ("animals" category) and phonetic fluency (words starting with letter P), both of which assess verbal productivity (Benton and Spreen, 1969); Trail Making Tests (TMT) A and B from which we derived TMT (A-B), which is the difference between Part B and Part A and provides a purer indicator of cognitive flexibility (Reitan and Wolfson, 1985); and the Stroop Test (inhibition) (Golden and Freshwater, 1978). In addition, the Beck Depression Inventory-II (BDI-II) (Beck et al., 1996) was administered to screen for presence

and severity of depressive symptoms. To estimate premorbid intelligence the Word Accentuation Test Buenos Aires version (WAT-BA) was administered (Burin et al., 2000) and IQ was estimated based upon its results (Sanjurjo et al., 2015). All tests were administered and scored by a trained neuropsychologist (CA) blind to participant group.

We studied the association between cognitive test scores vs. WM integrity metrics (FD, FA and MD) of the tract of interest performing Spearman's correlation analysis.

### 2.10. Structural T1 MRI and Amyloid PET analysis

Entire cortex analyses were performed to explore cortical thickness and volumetry in O-LOAD and CS groups. Statistical maps were generated using the command-line group analysis stream in FreeSurfer software. For subcortical regions, only volumetry measures were calculated. PET images were processed along with MRI volumetric T1 images. Once T1 images were processed, an analysis was performed using PETSurfer scripts obtaining the corresponding PET-PiB and PET-FDG intensity maps. Both analyses have been described in detail (Duarte-Abritta et al., 2018).

Spearman's correlation analysis was applied to study rank-ordered associations between WM metrics of the significant tract and: i) structural GM (thickness and volumetry) metrics and ii) PET metrics (PiB and FDG), in both cases we used brain regions involved in the anatomical connectome. This analysis was performed in MATLAB-R2014a. Results of all statistical analysis were considered significant at $p<0.05$.

## 3. Results

Our sample included 23 O-LOAD and 22 CS with no known family history of LOAD. As shown in Table 1, O-LOAD and CS were similar in terms of age, sex, educational attainment, estimated IQ, and cognitive test scores such as semantic and phonetic fluencies, TMT (A-B), and Stroop. All participants were cognitively asymptomatic, neuropsychological performance was within normal limits, and none met clinical criteria for mild cognitive impairment or AD or related dementias.

The intergroup comparison of FBA is shown in Figure 1. The tract that displays significant differences in fiber density (FD, the intra-axonal volume of a fiber bundle) at fixel scale involves the splenium of the corpus callosum and the right fornix. It is shown in three ways. In panel A), the color bar indicates 40% higher FD in the CS group versus the O-LOAD group. Panel B) shows the same tract colored by streamline orientations; and panel C) shows it on a sagittal slice of the right hemisphere. The other two metrics of FBA were not different between O-LOAD and CS groups.

Differences in derived-tensor metrics between O-LOAD and CS were assessed via 2-sample t-tests. Figure 2 shows significant differences between groups in FA and MD for the tract obtained from FBA. FA was greater and MD smaller in CS compared with O-LOAD. In addition, regarding the relationship between DTI-based and FBA measures, FA was positively correlated with FD (Spearman's r=0.6906, $p=5.3x10^{-4}$) while MD was inversely correlated with FD (Spearman's r=-0.7007, $p=4.1x10^{-4}$) in CS group only. In O-LOAD the correlation between FA and FD values approached significance (Spearman's r=0.3972, p=0.06).

Figure 3 displays the anatomical connectome that includes GM structures contributing fibers to the tract of interest defined in Figure 1. Most of the structures involve posterior neocortex and a series of cortical and subcortical structures participating of limbic circuits, namely, left medial orbitofrontal and middle temporal gyri; right insular cortex, thalamus, and hippocampus; and bilateral superior temporal gyri, precunei and superior parietal gyri (Figure 3).

Regarding the relationship between WM integrity measures and cognitive scores, we obtained that FA in the significant tract was inversely related to performance on the semantic fluency test among O-LOAD (r=-0.4251, p=0.0432). Similarly, there was a marginally significant correlation between FD and semantic fluency (r=-0.4097, p=0.0522). No significant correlations were found between measures of WM integrity and phonetic fluency, Stroop, and TMT (B-A).

Finally, Figures 4 and 5 display correlation matrices and linear fit by O-LOAD and CS for all significant Spearman's correlations among WM integrity metrics (FA, MD, and FD) of the tract of interest shown in Figure 1, GM measures (cortical thickness and GM volume), and PET measures (PiB and FDG). Among CS, greater FD was associated with higher amyloid deposition as shown by PET-PiB intensity signal (Figure 4, panel A) and larger volume (Figure 4, panel B) in the right thalamus and bilateral superior parietal gyri. Amyloid deposition in the right thalamus was also associated with more FA (Figure 5, panel B, left plot) and less MD (Figure 5, panel A, middle plot) in the tract of interest. The latter was directly related to metabolism in the right thalamus as well (Figure 5, panel A, left plot). In CS, FA was associated with right superior parietal gyrus volume (Figure 5, panel B, right plot). Among O-LOAD, greater FD was associated with greater amyloid deposition in the right hippocampus (Figure 4, panel A, right plot) and left precuneus thinning (Figure 4, panel C, right plot). MD in the tract of interest was related to right superior temporal gyrus thinning in O-LOAD (Figure 5, panel A, right plot).

## 4. Discussion

Middle aged O-LOAD display decreased anatomical connectivity involving the splenium of the corpus callosum and the right fornix, as assessed with FBA method, which can reveal more detailed information than a voxel-based approach when compared with CS. Our study highlights two important aspects of applying FBA. First, we improved statistical power by performing the entire fixel statistical analysis implemented in FBA. Second the method allowed us to obtain a voxel-associated tract with different fiber-bundle orientations otherwise not possible to assess with more conventional methods such as TBSS (Raffelt et al., 2015).

We assessed canonical tensor-derived metrics only in the area of the significant tract to avoid noisy data of whole-brain maps. O-LOAD show decreased FA and increased MD. These results are consistent with previous reports, describing areas such as the corpus callosum, cingulum (Bendlin et al., 2010), and fornix (Ringman et al., 2007) evidencing lower FA in preclinical AD subjects compared to CS. These abnormalities and decreased FD could be due to a lesser number of axons, less myelinated axons, or disrupted microstructure favoring the free diffusion of water across the membranes of such fibers.

Axon fibers in the splenium of the corpus callosum convey interhemispheric information between neocortical areas including posterior parietal cortices and precunei, whereas the right fornix is the main WM tract originating in the ipsilateral hippocampal archicortex (Martin, 2003). These regions have been uniformly considered among the earliest affected structures in LOAD, specifically those involving neurofibrillary tangles (amyloid deposition occurs initially in association with the neocortex; (Dubois et al., 2014; Montine et al., 2012)). That semantic fluency, a performance measure involving bihemispheric posterior temporal/parietal regions (Fama et al., 2000), is the only clinical feature associated with the tracts displaying intergroup differences, suggests that these changes in anatomical connectivity, although subtle, may bear clinical implications in early LOAD (Laatu et al., 2003).

To our knowledge, this is a first report describing detection of WM structural differences at fixel scale in middle-aged at-risk adults without cognitive symptoms or neuropsychological impairments detectable using common tests of neuropsychological performance. The average age of our participants (i.e., over one decade younger on average than the expected age at onset of clinical LOAD symptoms) precludes us from knowing if and how the detected WM differences are predictive of LOAD. However, if confirmed in larger samples followed over several years, these may represent very early biomarkers of the disease. As reported recently by our group (Duarte-Abritta et al., 2018), these O-LOAD do not exhibit significant mesial temporal atrophy, usually

considered the earliest structural brain imaging biomarker of LOAD (Dubois et al., 2014). This suggests that anatomical connectivity might reveal intracellular neurofibrillary differences ultimately affecting axons (Braak and Del Tredici, 2015; Montine et al., 2012), prior to the appearance of detectable neurodegeneration in the GM. This has been explored in clinical samples of LOAD patients through FBA (Mito et al., 2018) and the results are in line with our observations.

To obtain clues about the possible pathophysiological origins of observed differences, we correlated the magnitude of WM microstructure in O-LOAD and CS, and observed the presence of both regional amyloid deposition and neurodegeneration as assessed by GM volume, cortical thickness or regional cerebral metabolism. Resulting associations were different for O-LOAD vs CS. Among the latter, most correlations were observed for the right thalamus and bilateral superior parietal gyri. Indicators of greater WM abnormalities in the splenium and right fornix were related to decreased amyloid, decreased volume, and increased cerebral metabolism in the right thalamus, along with similar findings in either superior parietal gyrus. Our CS are comparable to post-mortem studies (Braak and Braak, 1991; Braak and Del Tredici, 2015), since we observe an association of integrity of fibers of the splenium with the right thalamus. By contrast, in O-LOAD, greater compromise of WM integrity (decreased FD) in the aforementioned tracts were associated with lower amyloid deposition in the right hippocampus and greater thickness in the left precuneus. These findings suggest a differential relationship between GM and WM integrity in both groups. Among O-LOAD, in contrast, the relationship involves GM structures traditionally associated with LOAD (Montine et al., 2012), lending further support to the idea that early WM differences in O-LOAD as described heremight be related to risk of AD.

One interpretation of our results may be that O-LOAD display an accelerated pathophysiological process involving AD-specific structures such as medial temporal lobes (including hippocampi) and precunei (Dubois et al., 2014; Montine et al., 2012), instead of thalamus. In light of these observations, the age-dependent progression from brainstem to limbic to neocortical involvement seen in neuropathological studies (Braak and Braak, 1991; Braak and Del Tredici, 2015) might not specifically precede LOAD, but reflect normal aging. In contrast, among O-LOAD, we see specific involvement of the right hippocampus and precunei, suggesting that intergroup differences are related to LOAD predisposition instead of “accelerated aging”. This is in line with very early observations of precuneus compromise in infants at risk for AD by virtue of their genetic risk (Dean et al., 2014), and in whom neurodegeneration would be unlikely at such an early age.

In contrast to our prediction, CS displayed a regional relationship between WM abnormalities and amyloid deposition, again in the right thalamus and left superior parietal gyrus. This may point to a general phenomenon of an amyloid-Tau protein relationship that is not necessarily related to risk of LOAD, but reflects normal aging. Further, beta-amyloid on PET imaging was inversely related to WM integrity in the studied tracts. As previously reported (Braak and Braak, 1991), amyloid deposition in structures initially affected by neurofibrillary changes (e.g., medial temporal lobes) is a late occurrence in LOAD. These observations are clearly contrary to a LOAD-related regional phenomenon whereby extracellular amyloid deposition and intercellular phosphorylated Tau accumulation coincide to produce neurodegeneration (Jack et al., 2010). Whereas long-term follow up of middle-aged adults would provide the best evidence on how our findings are related to development of LOAD, comparison between O-LOAD and CS comprised of a similar sociodemographic background factors, will likely provide significant insight into how anatomical connectivity constitutes an early biomarker of LOAD.

The present investigation has several limitations. Our sample was homogeneous regarding ethnicity, geographical area, culture, and years of education, perhaps limiting generalizability of the results. As per the acquisition protocol, the non-isotropic voxel size could introduce a bias during the tractography process, especially in the largest direction. Nonetheless, FBA implements techniques that increase statistical inference, and according to our analysis, the significant tract is not oversampled in the largest direction and therefore might not be influenced by this issue. Hence, the current results have significant implications for understanding the earliest pathogenesis of LOAD and is worthy of further research.

**Acknowledgments**

The authors would like to thank Centro de Cómputos de Alto Rendimiento (CeCAR), Facultad de Ciencias Exactas y Naturales, University of Buenos Aires, for granting use of computational resources, which allowed us to perform most of the analyses included in this work. SDG. SMS, CA, BDA and HB are doctoral fellows from CONICET.

**Funding sources**

This work was supported by a local government funding agency: Agencia de Promoción (FONCYT, MINCYT) PICT 2014-0633.

**Author contributions**

SMS, MFV and SMG developed the scientific project. SMS performed processing dMRI and FBA. BDA executed the PET analyses and CA analyzed neuropsychological data. GDP, HB and MNC analyzed the results. SMS, MFV and SMG wrote the first draft of the manuscript. All authors edited and approved the final manuscript.

**Declaration of interest**

Dr. Charles B. Nemeroff's disclosures are as follows:
Research/Grants:
National Institutes of Health (NIH), Stanley Medical Research Institute
Consulting (*last three years*):
Xhale, Takeda, Taisho Pharmaceutical Inc., Prismic Pharmaceuticals, Bracket (Clintara), Total Pain Solutions (TPS), Gerson Lehrman Group (GLG) Healthcare & Biomedical Council, Fortress Biotech, Sunovion Pharmaceuticals Inc., Sumitomo Dainippon Pharma, Janssen Research & Development LLC, Magstim, Inc., Navitor Pharmaceuticals, Inc., TC MSO, Inc., Intra-Cellular Therapies, Inc.
Stockholder:
Xhale, Celgene, Seattle Genetics, Abbvie, OPKO Health, Inc., Network Life Sciences Inc., Antares, BI Gen Holdings, Inc.
Scientific Advisory Boards:
American Foundation for Suicide Prevention (AFSP), Brain and Behavior Research Foundation (BBRF) (*formerly named National Alliance for Research on Schizophrenia and Depression* [*NARSAD*]), Xhale, Anxiety Disorders Association of America (ADAA), Skyland Trail, Bracket (Clintara), RiverMend Health LLC, Laureate Institute for Brain Research, Inc.
Board of Directors:
AFSP, Gratitude America, ADAA
Income sources or equity of $10,000 or more:
American Psychiatric Publishing, Xhale, Bracket (Clintara), CME Outfitters, Takeda
Patents:
Method and devices for transdermal delivery of lithium (*US 6,375,990B1*)
Method of assessing antidepressant drug therapy via transport inhibition of monoamine neurotransmitters by ex vivo assay (*US 7,148,027B2*)
Speakers Bureau:
None
All other authors have nothing to disclose nor have any potential conflicts of interest.

**References**

Abulafia, C., Loewenstein, D., Curiel-Cid, R., Duarte-Abritta, B., Sánchez, S.M., Vigo, D.E., Castro, M.N., Drucaroff, L.J., Vázquez, S., Sevlever, G., Nemeroff, C.B., Guinjoan, S.M., Villarreal, M.F., 2018. Brain Structural and Amyloid Correlates of Recovery From Semantic Interference in Cognitively Normal Individuals With or Without Family History of Late-Onset Alzheimer's Disease. JNP 31, 25–36. https://doi.org/10.1176/appi.neuropsych.17120355

Aizenstein, H.J., Nebes, R.D., Saxton, J.A., Price, J.C., Mathis, C.A., Tsopelas, N.D., Ziolko, S.K., James, J.A., Snitz, B.E., Houck, P.R., Bi, W., Cohen, A.D., Lopresti, B.J., DeKosky, S.T., Halligan, E.M., Klunk, W.E., 2008. Frequent Amyloid Deposition Without Significant Cognitive Impairment Among the Elderly. Arch Neurol 65, 1509–1517. https://doi.org/10.1001/archneur.65.11.1509

Andersson, J.L.R., Sotiropoulos, S.N., 2016. An integrated approach to correction for off-resonance effects and subject movement in diffusion MR imaging. NeuroImage 125, 1063–1078. https://doi.org/10.1016/j.neuroimage.2015.10.019

Ballard, C., O'Sullivan, M.J., 2013. Alzheimer disease and stroke: Cognitive and neuroimaging predictors of AD and stroke. Nature Reviews Neurology 9, 605–606. https://doi.org/10.1038/nrneurol.2013.215

Beck, Steer, Robert A., Brown, Gregory K., 1996. Beck depression inventory -II [WWW Document]. URL https://blog.naver.com/mistyeyed73/220427762670

Bendlin, B.B., Ries, M.L., Canu, E., Sodhi, A., Lazar, M., Alexander, A.L., Carlsson, C.M., Sager, M.A., Asthana, S., Johnson, S.C., 2010. White matter is altered with parental family history of Alzheimer's disease. Alzheimer's & Dementia 6, 394–403. https://doi.org/10.1016/j.jalz.2009.11.003

Benton, A.L., Spreen, O., 1969. Embedded Figures Test: Manual of instructions and norms. Department of Psychology, University of Victoria.

Bertram, L., Lill, C.M., Tanzi, R.E., 2010. The Genetics of Alzheimer Disease: Back to the Future. Neuron 68, 270–281. https://doi.org/10.1016/j.neuron.2010.10.013

Boyle, P.A., Yu, L., Leurgans, S.E., Wilson, R.S., Brookmeyer, R., Schneider, J.A., Bennett, D.A., 2019. Attributable risk of Alzheimer's dementia attributed to age-related neuropathologies. Annals of Neurology 85, 114–124. https://doi.org/10.1002/ana.25380

Bozzali, M., Falini, A., Franceschi, M., Cercignani, M., Zuffi, M., Scotti, G., Comi, G., Filippi, M., 2002. White matter damage in Alzheimer's disease assessed in vivo using diffusion tensor magnetic resonance imaging. Journal of Neurology, Neurosurgery & Psychiatry 72, 742–746. https://doi.org/10.1136/jnnp.72.6.742

Braak, H., Braak, E., 1991. Neuropathological stageing of Alzheimer-related changes. Acta Neuropathol 82, 239–259. https://doi.org/10.1007/BF00308809

Braak, H., Del Tredici, K., 2015. The preclinical phase of the pathological process underlying sporadic Alzheimer's disease. Brain 138, 2814–2833. https://doi.org/10.1093/brain/awv236

Buckner, R.L., Sepulcre, J., Talukdar, T., Krienen, F.M., Liu, H., Hedden, T., Andrews-Hanna, J.R., Sperling, R.A., Johnson, K.A., 2009. Cortical Hubs Revealed by Intrinsic Functional Connectivity: Mapping, Assessment of Stability, and Relation to Alzheimer's Disease. J. Neurosci. 29, 1860–1873. https://doi.org/10.1523/JNEUROSCI.5062-08.2009

Burin, D.I., Jorge, R.E., Arizaga, R.A., Paulsen, J.S., 2000. Estimation of Premorbid Intelligence: The Word Accentuation Test - Buenos Aires Version. Journal of Clinical and Experimental Neuropsychology 22, 677–685. https://doi.org/10.1076/1380-3395(200010)22:5;1-9;FT677

Dean, D.C., Jerskey, B.A., Chen, K., Protas, H., Thiyyagura, P., Roontiva, A., O'Muircheartaigh, J., Dirks, H., Waskiewicz, N., Lehman, K., Siniard, A.L., Turk, M.N., Hua, X., Madsen, S.K., Thompson, P.M., Fleisher, A.S., Huentelman, M.J., Deoni, S.C.L., Reiman, E.M., 2014. Brain Differences in Infants at Differential Genetic Risk for Late-Onset Alzheimer Disease: A Cross-sectional Imaging Study. JAMA Neurol 71, 11–22. https://doi.org/10.1001/jamaneurol.2013.4544

Desikan, R.S., Ségonne, F., Fischl, B., Quinn, B.T., Dickerson, B.C., Blacker, D., Buckner, R.L., Dale, A.M., Maguire, R.P., Hyman, B.T., Albert, M.S., Killiany, R.J., 2006. An automated labeling system for subdividing the human cerebral cortex on MRI scans into gyral based regions of interest. NeuroImage 31, 968–980. https://doi.org/10.1016/j.neuroimage.2006.01.021

Douaud, G., Jbabdi, S., Behrens, T.E.J., Menke, R.A., Gass, A., Monsch, A.U., Rao, A., Whitcher, B., Kindlmann, G., Matthews, P.M., Smith, S., 2011. DTI measures in crossing-fibre areas: Increased diffusion anisotropy reveals early white matter alteration in MCI and mild Alzheimer's disease. NeuroImage 55, 880–890. https://doi.org/10.1016/j.neuroimage.2010.12.008

Duarte-Abritta, B., Villarreal, M.F., Abulafia, C., Loewenstein, D., Curiel Cid, R.E., Castro, M.N., Surace, E., Sánchez, S.-M., Vigo, D.E., Vázquez, S., Nemeroff, C.B., Sevlever, G., Guinjoan, S.M., 2018. Cortical thickness, brain metabolic activity, and in vivo amyloid deposition in asymptomatic, middle-aged offspring of patients with late-onset Alzheimer's disease. Journal of Psychiatric Research 107, 11–18. https://doi.org/10.1016/j.jpsychires.2018.10.008

Dubois, B., Feldman, H.H., Jacova, C., Hampel, H., Molinuevo, J.L., Blennow, K., DeKosky, S.T., Gauthier, S., Selkoe, D., Bateman, R., Cappa, S., Crutch, S., Engelborghs, S., Frisoni, G.B., Fox, N.C., Galasko, D., Habert, M.-O., Jicha, G.A., Nordberg, A., Pasquier, F., Rabinovici, G., Robert, P., Rowe, C., Salloway, S., Sarazin, M., Epelbaum, S., de Souza, L.C., Vellas, B., Visser, P.J., Schneider, L., Stern, Y., Scheltens, P., Cummings, J.L., 2014. Advancing research diagnostic criteria for Alzheimer's disease: the IWG-2 criteria. The Lancet Neurology 13, 614–629. https://doi.org/10.1016/S1474-4422(14)70090-0

During, E.H., Osorio, R.S., Elahi, F.M., Mosconi, L., de Leon, M.J., 2011. The concept of FDG-PET endophenotype in Alzheimer's disease. Neurol Sci 32, 559–569. https://doi.org/10.1007/s10072-011-0633-1

Fama, R., Sullivan, E.V., Shear, P.K., Cahn-Weiner, D.A., Marsh, L., Lim, K.O., Yesavage, J.A., Tinklenberg, J.R., Pfefferbaum, A., 2000. Structural brain correlates of verbal and nonverbal fluency measures in Alzheimer's disease. Neuropsychology 14, 29–40. https://doi.org/10.1037/0894-4105.14.1.29

Ferrer, I., 2012. Defining Alzheimer as a common age-related neurodegenerative process not inevitably leading to dementia. Progress in Neurobiology 97, 38–51. https://doi.org/10.1016/j.pneurobio.2012.03.005

Golden, C.J., Freshwater, S.M., 1978. Stroop color and word test.

Greicius, M.D., Srivastava, G., Reiss, A.L., Menon, V., 2004. Default-mode network activity distinguishes Alzheimer's disease from healthy aging: Evidence from functional MRI. PNAS 101, 4637–4642. https://doi.org/10.1073/pnas.0308627101

Jack, C.R., Knopman, D.S., Jagust, W.J., Shaw, L.M., Aisen, P.S., Weiner, M.W., Petersen, R.C., Trojanowski, J.Q., 2010. Hypothetical model of dynamic biomarkers of the Alzheimer's pathological cascade. The Lancet Neurology 9, 119–128. https://doi.org/10.1016/S1474-4422(09)70299-6

Jeurissen, B., Leemans, A., Jones, D.K., Tournier, J.-D., Sijbers, J., 2011. Probabilistic fiber tracking using the residual bootstrap with constrained spherical deconvolution. Human Brain Mapping 32, 461–479. https://doi.org/10.1002/hbm.21032

Jeurissen, B., Leemans, A., Tournier, J.-D., Jones, D.K., Sijbers, J., 2013. Investigating the prevalence of complex fiber configurations in white matter tissue with diffusion magnetic resonance imaging. Human Brain Mapping 34, 2747–2766. https://doi.org/10.1002/hbm.22099

Jeurissen, B., Tournier, J.-D., Dhollander, T., Connelly, A., Sijbers, J., 2014. Multi-tissue constrained spherical deconvolution for improved analysis of multi-shell diffusion MRI data. NeuroImage 103, 411–426. https://doi.org/10.1016/j.neuroimage.2014.07.061

Jones, D.K., 2010. Challenges and limitations of quantifying brain connectivity in vivo with diffusion MRI. Imaging in Medicine 2, 341–355.

Jones, D.K., Knösche, T.R., Turner, R., 2013. White matter integrity, fiber count, and other fallacies: The do's and don'ts of diffusion MRI. NeuroImage 73, 239–254. https://doi.org/10.1016/j.neuroimage.2012.06.081

Kantarci, K., 2014. Fractional Anisotropy of the Fornix and Hippocampal Atrophy in Alzheimer's Disease. Front. Aging Neurosci. 6. https://doi.org/10.3389/fnagi.2014.00316

Laatu, S., Revonsuo, A., Jäykkä, H., Portin, R., Rinne, J.O., 2003. Visual object recognition in early Alzheimer's disease: deficits in semantic processing. Acta Neurologica Scandinavica 108, 82–89. https://doi.org/10.1034/j.1600-0404.2003.00097.x

Loewenstein, D.A., Curiel, R.E., Duara, R., Buschke, H., 2018. Novel Cognitive Paradigms for the Detection of Memory Impairment in Preclinical Alzheimer's Disease. Assessment 25, 348–359. https://doi.org/10.1177/1073191117691608

Loewenstein, D.A., Curiel, R.E., Greig, M.T., Bauer, R.M., Rosado, M., Bowers, D., Wicklund, M., Crocco, E., Pontecorvo, M., Joshi, A.D., Rodriguez, R., Barker, W.W., Hidalgo, J., Duara, R., 2016. A Novel Cognitive Stress Test for the Detection of Preclinical Alzheimer Disease: Discriminative Properties and Relation to Amyloid Load. The American Journal of Geriatric Psychiatry 24, 804–813. https://doi.org/10.1016/j.jagp.2016.02.056

Martin, J.H., 2003. Lymbic system and cerebral circuits for emotions, learning, and memory. Neuroanatomy: text and atlas (third ed.). McGraw-Hill Companies 382.

Mayo, C.D., Mazerolle, E.L., Ritchie, L., Fisk, J.D., Gawryluk, J.R., 2017. Longitudinal changes in microstructural white matter metrics in Alzheimer's disease. NeuroImage: Clinical 13, 330–338. https://doi.org/10.1016/j.nicl.2016.12.012

Mito, R., Raffelt, D., Dhollander, T., Vaughan, D.N., Tournier, J.-D., Salvado, O., Brodtmann, A., Rowe, C.C., Villemagne, V.L., Connelly, A., 2018. Fibre-specific white matter reductions in Alzheimer's disease and mild cognitive impairment. Brain 141, 888–902. https://doi.org/10.1093/brain/awx355

Montine, T.J., Phelps, C.H., Beach, T.G., Bigio, E.H., Cairns, N.J., Dickson, D.W., Duyckaerts, C., Frosch, M.P., Masliah, E., Mirra, S.S., 2012. National Institute on Aging; Alzheimer's Association. National Institute on Aging-Alzheimer's Association guidelines for the neuropathologic assessment of Alzheimer's disease: a practical approach. Acta Neuropathol 123, 1–11.

Mosconi, L., Berti, V., Swerdlow, R.H., Pupi, A., Duara, R., de Leon, M., 2010. Maternal transmission of Alzheimer's disease: Prodromal metabolic phenotype and the search for genes. Human Genomics 4, 170. https://doi.org/10.1186/1479-7364-4-3-170

Mosconi, L., Murray, J., Tsui, W.H., Li, Y., Spector, N., Goldowsky, A., Williams, S., Osorio, R., McHugh, P., Glodzik, L., Vallabhajosula, S., de Leon, M.J., 2014. Brain imaging of cognitively normal individuals with 2 parents affected by late-onset AD. Neurology 82, 752–760. https://doi.org/10.1212/WNL.0000000000000181

Mosconi, L., Rinne, J.O., Tsui, W.H., Murray, J., Li, Y., Glodzik, L., McHugh, P., Williams, S., Cummings, M., Pirraglia, E., Goldsmith, S.J., Vallabhajosula, S., Scheinin, N., Viljanen, T., Någren, K., de Leon, M.J., 2013. Amyloid and metabolic positron emission tomography imaging of cognitively normal adults with Alzheimer's parents. Neurobiology of Aging 34, 22–34. https://doi.org/10.1016/j.neurobiolaging.2012.03.002

Ouyang, X., Chen, K., Yao, L., Hu, B., Wu, X., Ye, Q., Guo, X., 2015. Simultaneous changes in gray matter volume and white matter fractional anisotropy in Alzheimer's disease revealed by multimodal CCA and joint ICA. Neuroscience 301, 553–562. https://doi.org/10.1016/j.neuroscience.2015.06.031

Patenaude, B., Smith, S.M., Kennedy, D.N., Jenkinson, M., 2011. A Bayesian model of shape and appearance for subcortical brain segmentation. NeuroImage 56, 907–922. https://doi.org/10.1016/j.neuroimage.2011.02.046

Pierpaoli, C., Barnett, A., Pajevic, S., Chen, R., Penix, L., Virta, A., Basser, P., 2001. Water Diffusion Changes in Wallerian Degeneration and Their Dependence on White Matter Architecture. NeuroImage 13, 1174–1185. https://doi.org/10.1006/nimg.2001.0765

Pierpaoli, C., Basser, P.J., 1996. Toward a quantitative assessment of diffusion anisotropy. Magnetic Resonance in Medicine 36, 893–906. https://doi.org/10.1002/mrm.1910360612

Racine, A.M., Adluru, N., Alexander, A.L., Christian, B.T., Okonkwo, O.C., Oh, J., Cleary, C.A., Birdsill, A., Hillmer, A.T., Murali, D., Barnhart, T.E., Gallagher, C.L., Carlsson, C.M., Rowley, H.A., Dowling, N.M., Asthana, S., Sager, M.A., Bendlin, B.B., Johnson, S.C., 2014. Associations between white matter microstructure and amyloid burden in preclinical Alzheimer's disease: A multimodal imaging investigation. NeuroImage: Clinical 4, 604–614. https://doi.org/10.1016/j.nicl.2014.02.001

Raffelt, D.A., Smith, R.E., Ridgway, G.R., Tournier, J.-D., Vaughan, D.N., Rose, S., Henderson, R., Connelly, A., 2015. Connectivity-based fixel enhancement: Whole-brain statistical analysis of diffusion MRI measures in the presence of crossing fibres. NeuroImage 117, 40–55. https://doi.org/10.1016/j.neuroimage.2015.05.039

Raffelt, D.A., Tournier, J.-D., Smith, R.E., Vaughan, D.N., Jackson, G., Ridgway, G.R., Connelly, A., 2017. Investigating white matter fibre density and morphology using fixel-based analysis. NeuroImage 144, 58–73. https://doi.org/10.1016/j.neuroimage.2016.09.029

Rapp, M.A., Reischies, F.M., 2005. Attention and Executive Control Predict Alzheimer Disease in Late Life: Results From the Berlin Aging Study (BASE). The American Journal of Geriatric Psychiatry 13, 134–141. https://doi.org/10.1097/00019442-200502000-00007

Reiman, E.M., Chen, K., Alexander, G.E., Caselli, R.J., Bandy, D., Osborne, D., Saunders, A.M., Hardy, J., 2005. Correlations between apolipoprotein E ε4 gene dose and brain-imaging measurements of regional hypometabolism. PNAS 102, 8299–8302. https://doi.org/10.1073/pnas.0500579102

Reinvang, I., Grambaite, R., Espeseth, T., 2012. Executive Dysfunction in MCI: Subtype or Early Symptom [WWW Document]. International Journal of Alzheimer's Disease. https://doi.org/10.1155/2012/936272

Reitan, R.M., Wolfson, D., 1985. The Halstead-Reitan neuropsychological test battery: Theory and clinical interpretation. Reitan Neuropsychology.

Ringman, J.M., O'Neill, J., Geschwind, D., Medina, L., Apostolova, L.G., Rodriguez, Y., Schaffer, B., Varpetian, A., Tseng, B., Ortiz, F., Fitten, J., Cummings, J.L., Bartzokis, G., 2007. Diffusion tensor imaging in preclinical and presymptomatic carriers of familial Alzheimer's disease mutations. Brain 130, 1767–1776. https://doi.org/10.1093/brain/awm102

Rodrigue, K.M., Kennedy, K.M., Devous, M.D., Rieck, J.R., Hebrank, A.C., Diaz-Arrastia, R., Mathews, D., Park, D.C., 2012. β-Amyloid burden in healthy aging: regional distribution and cognitive consequences. Neurology 78, 387–395.

Rowe, C.C., Ellis, K.A., Rimajova, M., Bourgeat, P., Pike, K.E., Jones, G., Fripp, J., Tochon-Danguy, H., Morandeau, L., O'Keefe, G., Price, R., Raniga, P., Robins, P., Acosta, O., Lenzo, N., Szoeke, C., Salvado, O., Head, R., Martins, R., Masters, C.L., Ames, D., Villemagne, V.L., 2010. Amyloid imaging results from the Australian Imaging, Biomarkers and Lifestyle (AIBL) study of aging. Neurobiology of Aging, Alzheimer's Disease Neuroimaging Initiative (ADNI) Studies 31, 1275–1283. https://doi.org/10.1016/j.neurobiolaging.2010.04.007

Sánchez, S.M., Abulafia, C., Duarte-Abritta, B., de Guevara, M.S.L., Castro, M.N., Drucaroff, L., Sevlever, G., Nemeroff, C.B., Vigo, D.E., Loewenstein, D.A., Villarreal, M.F., Guinjoan, S.M., 2017. Failure to Recover from Proactive Semantic Interference and Abnormal Limbic Connectivity in Asymptomatic, Middle-Aged Offspring of Patients with Late-Onset Alzheimer's Disease. Journal of Alzheimer's Disease 60, 1183–1193. https://doi.org/10.3233/JAD-170491

Sanjurjo, N.S., Montañes, P., Matamoros, F.A.S., Burin, D., 2015. Estimating Intelligence in Spanish: Regression Equations With the Word Accentuation Test and Demographic Variables in Latin America. Applied Neuropsychology: Adult 22, 252–261. https://doi.org/10.1080/23279095.2014.918543

Sheline, Y.I., Raichle, M.E., 2013. Resting State Functional Connectivity in Preclinical Alzheimer's Disease. Biological Psychiatry, Alzheimer's Disease: From Neuropathology to Deficits in Functional Connectivity 74, 340–347. https://doi.org/10.1016/j.biopsych.2012.11.028

Sheng, C., Xia, M., Yu, H., Huang, Y., Lu, Y., Liu, F., He, Y., Han, Y., 2017. Abnormal global functional network connectivity and its relationship to medial temporal atrophy in patients with amnestic mild cognitive impairment. PLOS ONE 12, e0179823. https://doi.org/10.1371/journal.pone.0179823

Smith, R.E., Tournier, J.-D., Calamante, F., Connelly, A., 2015. SIFT2: Enabling dense quantitative assessment of brain white matter connectivity using streamlines tractography. NeuroImage 119, 338–351. https://doi.org/10.1016/j.neuroimage.2015.06.092

Smith, R.E., Tournier, J.-D., Calamante, F., Connelly, A., 2013. SIFT: Spherical-deconvolution informed filtering of tractograms. NeuroImage 67, 298–312. https://doi.org/10.1016/j.neuroimage.2012.11.049

Smith, S.M., 2002. Fast robust automated brain extraction. Human Brain Mapping 17, 143–155. https://doi.org/10.1002/hbm.10062

Smith, S.M., Jenkinson, M., Woolrich, M.W., Beckmann, C.F., Behrens, T.E.J., Johansen-Berg, H., Bannister, P.R., De Luca, M., Drobnjak, I., Flitney, D.E., Niazy, R.K., Saunders, J., Vickers, J., Zhang, Y., De Stefano, N., Brady, J.M., Matthews, P.M., 2004. Advances in functional and structural MR image analysis and implementation as FSL. NeuroImage, Mathematics in Brain Imaging 23, S208–S219. https://doi.org/10.1016/j.neuroimage.2004.07.051Tournier, J.-D., Calamante, F., Connelly, A., 2012. MRtrix: Diffusion tractography in crossing fiber regions. International Journal of Imaging Systems and Technology 22, 53–66. https://doi.org/10.1002/ima.22005

Tournier, J.-D., Calamante, F., Connelly, A., 2007. Robust determination of the fibre orientation distribution in diffusion MRI: Non-negativity constrained super-resolved spherical deconvolution. NeuroImage 35, 1459–1472. https://doi.org/10.1016/j.neuroimage.2007.02.016

Veraart, J., Novikov, D.S., Christiaens, D., Ades-aron, B., Sijbers, J., Fieremans, E., 2016. Denoising of diffusion MRI using random matrix theory. NeuroImage 142, 394–406. https://doi.org/10.1016/j.neuroimage.2016.08.016

Zhang, Y., Brady, M., Smith, S., 2001. Segmentation of brain MR images through a hidden Markov random field model and the expectation-maximization algorithm. IEEE Transactions on Medical Imaging 20, 45–57. https://doi.org/10.1109/42.906424

**Figure 1 White matter tract with significant differences in fiber density** Panel A) shows streamlines colored by percentage effect decrease in O-LOAD group respect of CS group. Panel B) depicts the same tract colored according the streamline orientations: left-right in red, anterior-posterior in green, and superior-inferior in blue. Panel C) shows the tract on a sagittal slice of the right hemisphere. In all panels the tract is displayed on a population template image.

**Figure 2 Significant differences in FA and MD** FA and MD calculated in the tract defined in Figure 1, present statistically differences between CS and O-LOAD groups. * $p<0.05$.

**Figure 3 Gray matter areas involved in connections of the tract** This connectome displayed gray matter regions connected through the tract defined in Figure 1. Each white matter connection is represented by a single link.

**Figure 4 Scatter plots of MRI and PET data vs FD** Each scatter plot shows the distribution of PIB data (panel A), and gray matter volume (panel B) or thickness (panel C) for specific regions vs. FD of CS (blue empty markers) and O-LOAD (orange empty markers) groups. When a Spearman's correlation is statistically significant ($p<0.05$), its linear fit is added for this group and the empty markers are filled. Statistically significant p-values and correlation coefficients are reported.

**Figure 5 Scatter plots of MRI and PET data vs tensor-derived metrics** Each scatter plot displays the data distribution of MRI and PET metrics versus MD (panel A) and FA (panel B) of CS (blue empty markers) and O-LOAD (orange empty markers) group. When a Spearman's correlation is statistically significant ($p<0.05$), its linear fit is added for this group and the empty markers are filled. Statistically significant p-values and correlation coefficients are reported.

**Declaration of interest**

Dr. Charles B. Nemeroff's disclosures are as follows:

Research/Grants:

National Institutes of Health (NIH), Stanley Medical Research Institute

Consulting (*last three years*):

Xhale, Takeda, Taisho Pharmaceutical Inc., Prismic Pharmaceuticals, Bracket (Clintara), Total Pain Solutions (TPS), Gerson Lehrman Group (GLG) Healthcare & Biomedical Council, Fortress Biotech, Sunovion Pharmaceuticals Inc., Sumitomo Dainippon Pharma, Janssen Research & Development LLC, Magstim, Inc., Navitor Pharmaceuticals, Inc., TC MSO, Inc., Intra-Cellular Therapies, Inc.

Stockholder:

Xhale, Celgene, Seattle Genetics, Abbvie, OPKO Health, Inc., Network Life Sciences Inc., Antares, BI Gen Holdings, Inc.

Scientific Advisory Boards:

American Foundation for Suicide Prevention (AFSP), Brain and Behavior Research Foundation (BBRF) (*formerly named National Alliance for Research on Schizophrenia and Depression* [*NARSAD*]), Xhale, Anxiety Disorders Association of America (ADAA), Skyland Trail, Bracket (Clintara), RiverMend Health LLC, Laureate Institute for Brain Research, Inc.

Board of Directors:

AFSP, Gratitude America, ADAA

Income sources or equity of $10,000 or more:

American Psychiatric Publishing, Xhale, Bracket (Clintara), CME Outfitters, Takeda

Patents:

Method and devices for transdermal delivery of lithium (*US 6,375,990B1*)

Method of assessing antidepressant drug therapy via transport inhibition of monoamine neurotransmitters by ex vivo assay (*US 7,148,027B2*)

Speakers Bureau:

None

All other authors have nothing to disclose nor have any potential conflicts of interest.

**Highlights**

- Healthy offspring of late-onset AD (O-LOAD) patients show decreased connectivity
- Gray matter anomalies are associated to altered white matter integrity among O-LOAD
- White matter dysconnectivity involves right fornix and splenium of corpus callosum

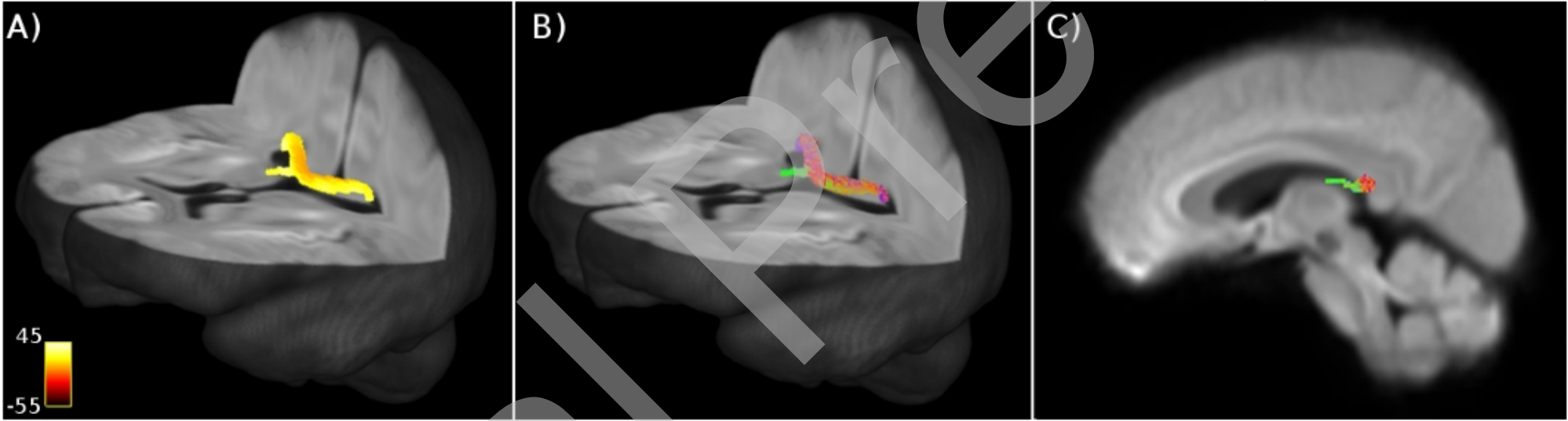
A)
B)
C)
45
-55

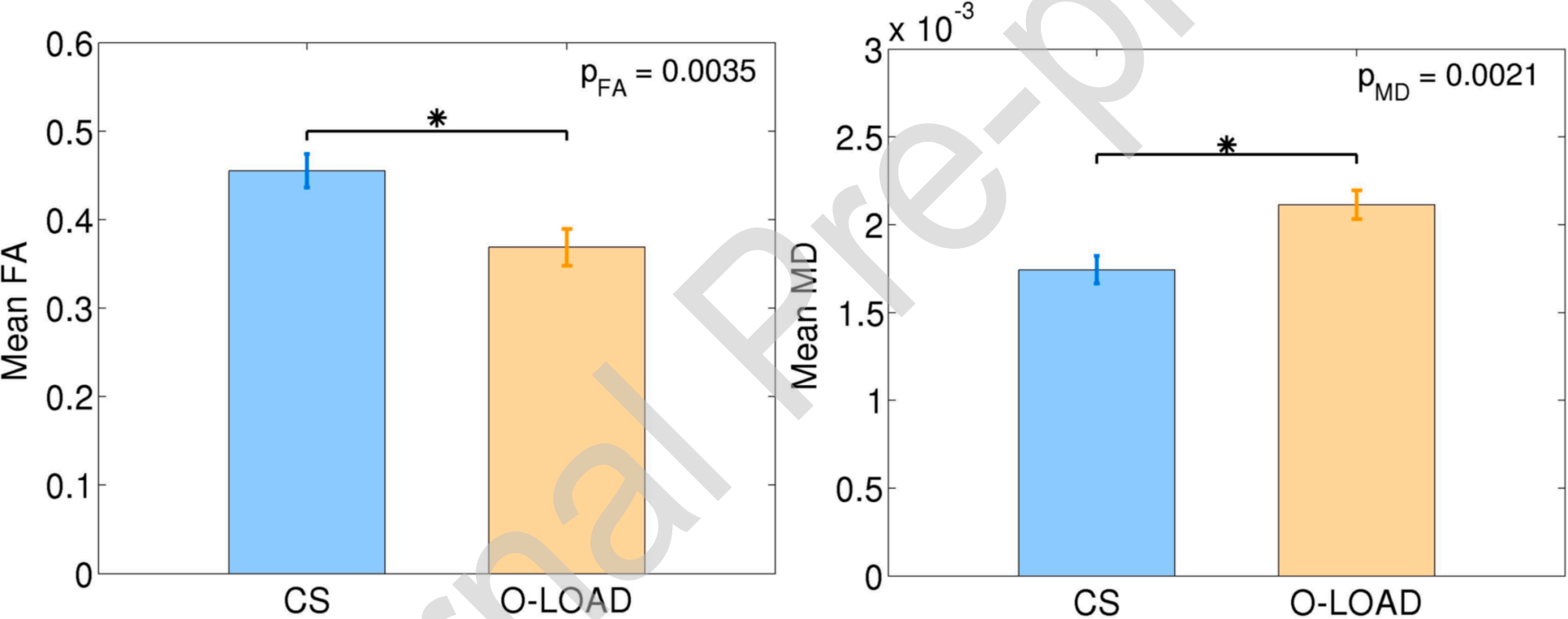

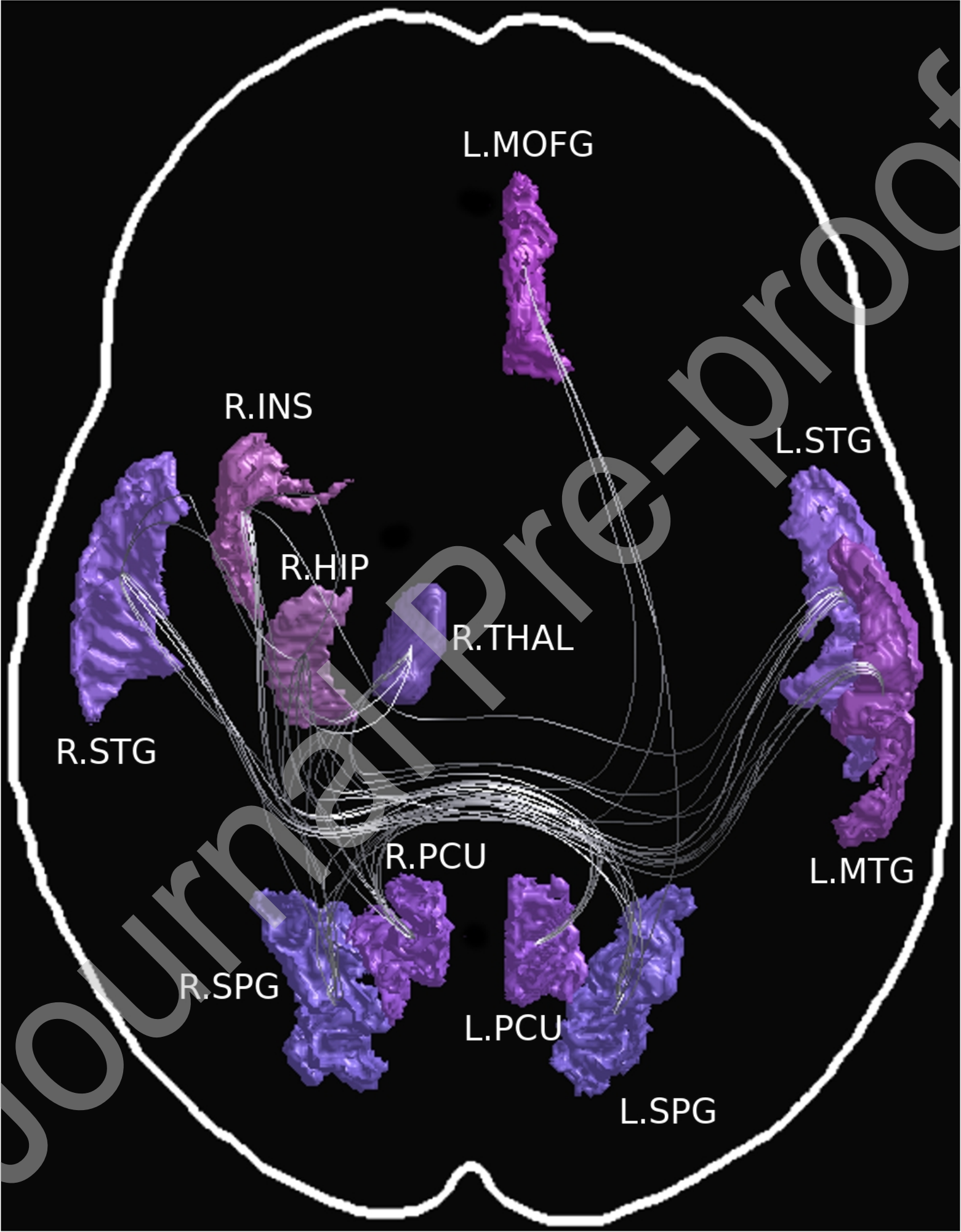

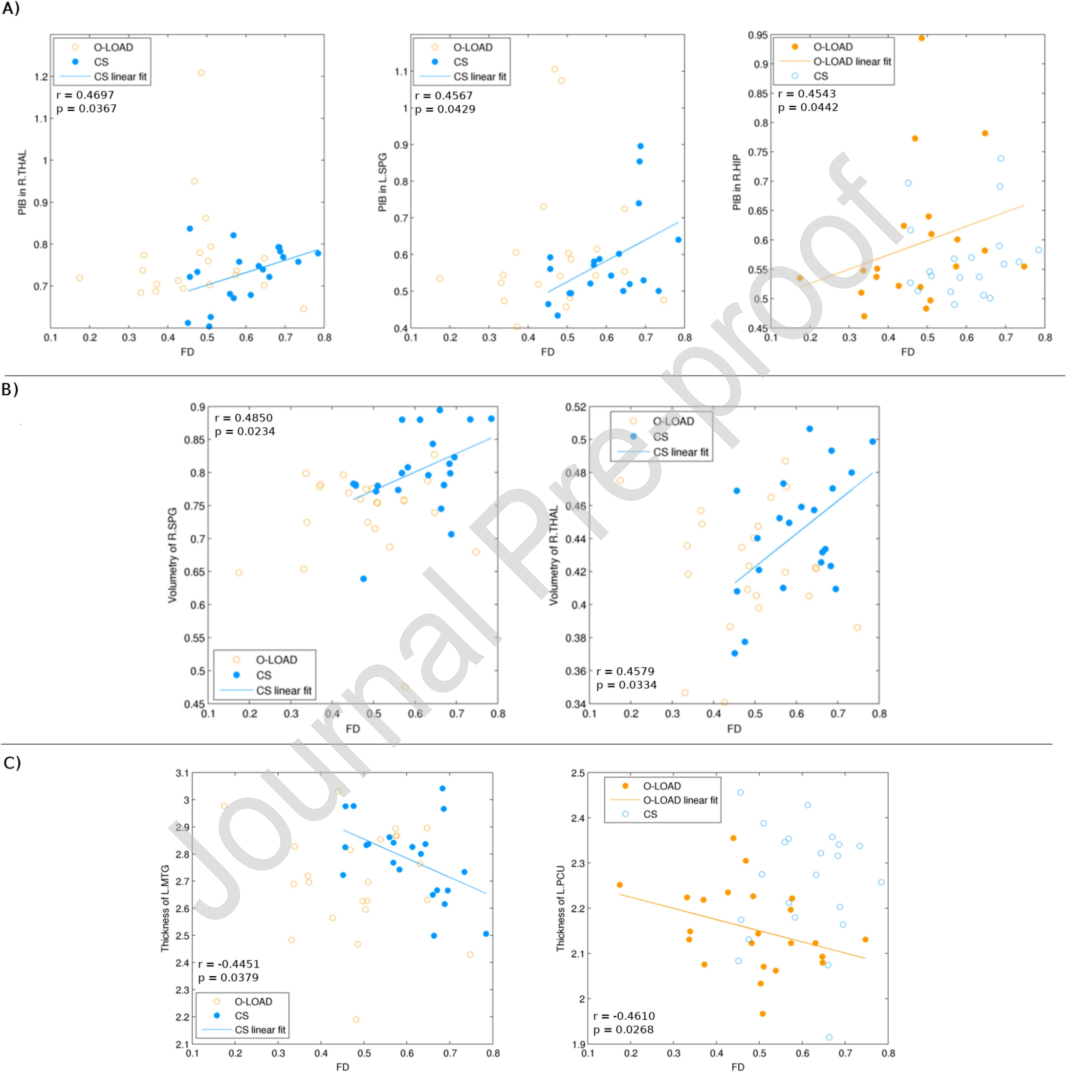

A)

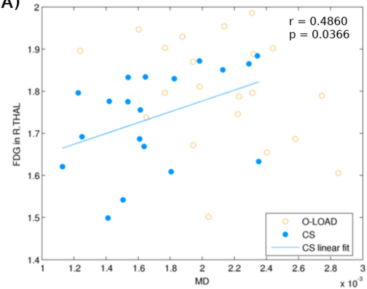


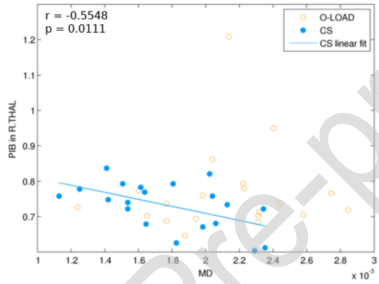


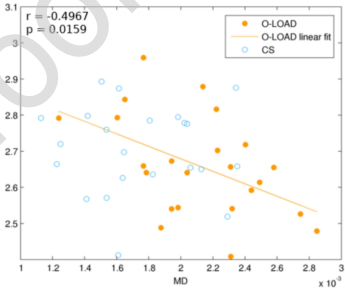


B)

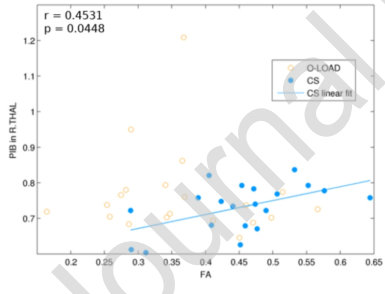


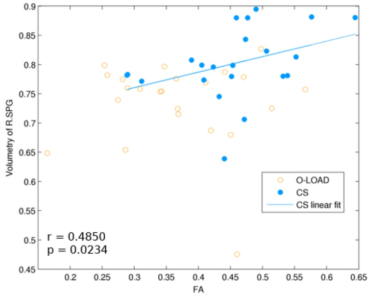

**Table 1. Demographic and clinical data**

| | Group | | | | | |
|---|---|---|---|---|---|---|
| | CS (n=22) | | O-LOAD (n=23) | | Statistic | p |
| | Mean or Frequency | SD or % | Mean or Frequency | SD or % | | |
| Female | 18.0 | 81.8 | 15.0 | 65.2 | $X^2$= 1.585 | .208 |
| Age | 51.91 | 6.46 | 54.91 | 5.37 | T= -1.693 | .100 |
| Education | 17.68 | 2.44 | 17.70 | 3.34 | T= -.016 | .987 |
| BDI II | 8.60 | 7.85 | 7.00 | 5.70 | T= .744 | .462 |
| Estimated IQ | 107.80 | 5.91 | 106.72 | 5.43 | T= .633 | .530 |
| Semantic Fluency | 22.05 | 4.85 | 20.74 | 3.79 | T= .990 | .328 |
| Phonetic Fluency | 18.10 | 4.01 | 18.17 | 4.04 | T= -.065 | .949 |
| TMT B-A | 34.90 | 13.94 | 37.24 | 14.22 | T= -.537 | .594 |
| Stroop | 2.86 | 8.14 | 3.38 | 6.39 | T= -.214 | .832 |

BDI II: Beck Depression Inventory, second version; TMT B-A: Trail Making Test A and B. T test was used for numeric variables and chi square test for categorical variables.